Carcinoma-associated fibroblast-derived lysyl oxidase-rich extracellular vesicles mediate collagen crosslinking and promote epithelial-mesenchymal transition

Xue Liu
Shanghai Stomatological Hospital, Fudan University
Jiao Li
Shanghai Stomatological Hospital, Fudan University
Xuesong Yang
Dalian Medical University
Xiaojie Li
Dalian Medical University
Jing Kong
Dalian Medical University
Dongyuan Qi
the First Affiliated Hospital of Dalian Medical University
Fuyin Zhang
the Second Affiliated Hospital of Dalian Medical University
Bo Sun
the Second Affiliated Hospital of Dalian Medical University
Yuehua Liu
Shanghai Stomatological Hospital, Fudan University
Tingjiao Liu (tingjiao_liu@fudan.edu.cn)
Shanghai Stomatological Hospital, Fudan University

Research Article

Keywords: Carcinoma-associated fibroblasts, small extracellular vesicles, LOX, collagen crosslinking, epithelial-mesenchymal transition

Posted Date: February 16th, 2022

DOI: https://doi.org/10.21203/rs.3.rs-1352348/v1

Abstract

Background: Carcinoma-associated fibroblasts (CAFs) are the main cellular components of the tumor microenvironment and promote cancer progression by modifying the extracellular matrix (ECM). The tumor-associated ECM is characterized by collagen crosslinking catalyzed by lysyl oxidase (LOX). Small extracellular vesicles (sEVs) mediate cell-cell communication. However, the interactions between sEVs and the ECM remain unclear.

Methods: sEVs separation was performed by differential ultracentrifugation. Normal fibroblasts (NFs) were treated with sEVs and the content of collagen crosslinking were performed by ELISA. Active LOX (αLOX) was enriched in sEVs were performed by western blot and ELISA. TCI-15 was used to inhibited sEVs bind to collagen I and triggered collagen crosslinking. CAF sEV-induced collagen crosslinking promoted the epithelial-mesenchymal transition (EMT) of OSCC cells was confirmed both in vitro and in vivo.

Results: Here, we demonstrate, for the first time, that sEVs released from oral squamous cell carcinoma (OSCC)-derived CAFs induce collagen crosslinking, thereby promoting EMT. CAF sEVs preferably bound to the ECM rather than being taken up by fibroblasts and induced collagen crosslinking, and a LOX inhibitor or blocking antibody suppressed this effect. αLOX, but not the LOX precursor, was enriched in CAF sEVs and interacted with periostin, fibronectin, and bone morphogenetic protein-1 on the surface of sEVs. CAF sEV-associated integrin α2β1 mediated the binding of CAF sEVs to collagen I, and blocking integrin α2β1 inhibited collagen crosslinking by interfering with CAF sEV binding to collagen I. CAF sEV-induced collagen crosslinking promoted the EMT of OSCC cells in vitro and in vivo.

Conclusions: This work reveals that CAF sEV-αLOX interacted with FN, POSTN, and BMP-1 on the surface of sEVs. Integrin α2β1 mediated the binding of CAF sEVs to collagen I, and αLOX triggered collagen crosslinking directly. Collagen crosslinking induced by CAF sEVs promoted the EMT of OSCC cells.

Background

Carcinoma-associated fibroblasts (CAFs) are often referred to as activated fibroblasts and they are abundant in the tumor stroma [1]. CAFs have important functions, including the deposition of extracellular matrix (ECM) constituents and the regulation of tumor cell proliferation and invasion [2, 3]. Collagen, the most abundant ECM component, provides structural integrity and tensile strength to human tissues [4, 5]. The tumor-associated ECM is characterized by collagen crosslinking that provides stability by assembling collagen into thick fibers, thereby increasing the stiffness of the ECM [6, 7]. Increased ECM stiffness is present in various cancers and stimulates epithelial–mesenchymal transition (EMT) of cancer cells [8-12]. However, the mechanisms by which CAFs drive collagen crosslinking and thus affect tumor cells remain to be fully elucidated.

Lysyl oxidase (LOX) catalyzes the crosslinking of collagen fibrils to form structurally stable collagen I fibers [13-15]. Collagen initially forms immature crosslinks including dihydroxylysino-norleucine (DHLNL)

and hydroxylysino-norleucine (HLNL). These immature forms react with another telopeptide residue to form mature crosslinks such as pyridinoline (PYD) [6, 16, 17]. LOX is synthesized as a preproenzyme containing an N-terminal signal peptide sequence, a propeptide, and a catalytic domain. The signal peptide is removed intracellularly to generate proLOX, which contains the propeptide and the catalytic domain [18, 19]. The propeptide is required for the exit of proLOX from the endoplasmic reticulum. The proLOX is processed extracellularly by bone morphogenetic protein-1 (BMP-1), resulting in the release of the catalytic domain, a biologically active form of LOX (αLOX) [20, 21]. Periostin (POSTN), a secretory protein expressed in collagen rich fibrous tissues, provides a specific microenvironment to regulate LOX catalytic activity [22, 23]. POSTN is composed of three domains: an amino-terminal EMI domain that interacts with fibronectin (FN), a tandem repeat of four FAS1 domains that bind to BMP-1, and a carboxyl-terminal domain [22, 23]. POSTN recruits BMP-1 onto the FN matrix to enhance LOX activity for collagen crosslinking [24]. Extracellular vesicles (EVs) have attracted considerable attention because of their capacity for carrying proteins, lipids, and nucleic acids and transferring their cargo to recipient cells [25-27]. EVs are classified into two main categories according to their biogenesis: exosomes and microvesicles [28]. Exosomes are produced through the fusion of multivesicular bodies with the plasma membrane [29], whereas microvesicles are secreted by plasma membrane shedding [30, 31]. In cases in which the intercellular origin of EVs is unknown, size-based EV nomenclature is used as follows: EVs smaller than 200 nm in diameter are defined as small EVs (sEVs), whereas EVs between 200 and 1000 nm in diameter are defined as large EVs [32]. The role of sEVs in mediating cell-cell communications has been demonstrated; however, whether sEVs mediate the communication between cells and the ECM remains unclear [33,34].

In this study, we isolated primary CAFs from human oral squamous cell carcinoma (OSCC) specimens to investigate the role of CAF-derived sEVs in ECM remodeling. We demonstrated that αLOX interacts with POSTN and BMP-1 on the surface of CAF sEVs. The sEV-associated αLOX was enzymatically active and induced collagen crosslinking directly. In addition, we verified that CAF sEVs detect collagen I via their surface receptor integrin α2β1. The results indicate that sEV-αLOX promotes collagen crosslinking, thereby inducing EMT in OSCC.

Results

CAF sEVs bind to the ECM and mediate collagen crosslinking

CAFs were isolated from the tissue samples of human OSCC cases. The characteristics of CAFs and their sEVs were shown in Figure S1. These cells express typical biomarkers of activated fibroblasts, including vimentin, FSP-1, FAP, and α-SMA, and do not express pan-cytokeratin, an epithelial biomarker (Figure S1a, 1b). Positive expression of LOX, which regulates collagen crosslinking, was detected in CAF-S1/S2/S3/S4 cells (Figure S1a). CAF CM increased the proliferation and migration abilities of UM-SCC6 cells compared with NF CM (Figure S1c, 1d).

CAF-S1/S2/S3/S4 and UM-SCC6 sEVs were isolated from the respective CM by ultracentrifugation (Figure S2a) and showed the typical morphology of exosomes in TEM images (Figure S2b). They were positive for sEV biomarkers, including CD63, CD9, and HSP-70, and negative for CALNEXIN, a biomarker of the endoplasmic reticulum (Figure S2c). The size distribution and particle concentration of sEVs were measured using a nanoparticle tracing system. The average size of these sEVs was approximately 130 nm, and there were approximately 5×10^7 sEVs per 1 mL CM (Figure S2d).

To determine whether CAF sEVs interact with the ECM, two experiments were designed. In the first experiment, NFs were seeded in a 12-well plate and cultured for 12 h to allow cells to fully adhere to the wall while producing a small amount of ECM. Then, PKH67-labeled CAF sEVs were added into each well and cultured for another 12 h (Figure 1a). In the second experiment, NFs were cultured for 72 h to induce the production of a large amount of ECM, followed by incubation with PKH67-labeled sEVs for 12 h (Figure 1b). In the first experimental group, CAF-S1/S2/S3/S4 sEVs were internalized into NFs in large numbers (Figure 1a). By contrast, in the second experimental group, CAF-S1/S2/S3/S4 sEVs were mostly located extracellularly and bound to the ECM instead of being uptaken by NFs (Figure 1b). Compared to CAF sEVs, the affinity of OSCC-derived sEVs to ECM is low (Figure S3). These findings indicate that CAF sEVs preferentially bind to the ECM when sufficient ECM is present.

Next, we analyzed the effect of CAF sEV binding on the ECM. NFs were cultured for 72 h and then incubated with CAF-S1/S2/S3/S4 sEVs for 12 h. To assess collagen crosslinking, we measured the levels of mature (PYD) and immature (DHLNL and HLNL) collagen crosslinks. PYD, DHLNL, and HLNL levels were significantly higher in the glucose and CAF-S1/S2/S3/S4 sEV groups than in the PBS-treated group (Figure 1c). Treatment with the LOX inhibitor BAPN or a LOX blocking antibody decreased the levels of PYD, DHLNL, and HLNL, especially the levels of the mature collagen crosslink PYD induced by the four types of CAF sEVs. These findings indicate that CAF sEVs induce collagen crosslinking, and CAF sEV-associated LOX plays an important role in this process.

CAFs release sEVs rich in αLOX on the surface

The expression of LOX in CAFs and CAF-derived sEVs was examined by western blotting. Both proLOX (50 kDa) and αLOX (32 kDa) were detected in CAF-S1/S2/S3/S4 cells, whereas only αLOX was detected in CAF-S1/S2/S3/S4 sEVs (Figure 2a). ProLOX and αLOX were not detected in sEV-depleted CM.
An immunogold labeling assay was performed to examine the association of αLOX with CAF sEVs. CD63 and CD9 served as the controls for sEV surface proteins. The results showed that CD63, CD9, and LOX proteins were present on the surface of CAF-S1/S2/S3/S4 sEVs (Figure 2b). The concentration of sEV-associated LOX (sEV-LOX) was determined by ELISA using intact CAF-S1/S2/S3/S4 sEVs. The concentration of sEV-LOX in CAF-S1/S2/S3/S4 cells increased in a sEV concentration-dependent manner (Figure 2c), and treatment with LOX blocking antibody significantly decreased the detectable sEV-LOX concentration. The concentration of CAF-S1/S2/S3/S4 sEV-LOX was approximately 0.15 ng/μg sEVs. These findings suggest that αLOX is located on the surface of CAF sEVs.

αLOX interacts with FN, POSTN, and BMP-1 on the surface of CAF sEVs

Next, we investigated how αLOX is located on the surface of CAF sEVs. POSTN binds to FN and recruits BMP-1 to the matrix, where BMP-1 cleaves pro-LOX to release αLOX. FN is one of the most extensively studied ECM molecules with respect to surface interaction with EVs [36]. We hypothesized that αLOX may be associated with sEVs by FN (Figure 3a). The expression of FN, POSTN, and BMP-1 in CAF-S1/S2/S3/S4 cells and their sEVs was confirmed by western blotting (Figure 3a). Immunoprecipitation assays confirmed that POSTN interacted with FN, BMP-1, and αLOX on CAF-S1/S2/S3/S4 sEVs (Figure 3b).

The results of ELISA demonstrated that the levels of POSTN in CAF-S1/S2/S3/S4 sEVs increased significantly in a sEV concentration-dependent manner, and treatment with a POSTN-blocking antibody interfered with POSTN detection (Figure 4a). CAF sEV-associated POSTN was approximately 0.02 ng per 1 μg sEVs. Next, CAF-S1/S2/S3/S4 were transfected with si-POSTN-1 and si-POSTN-2 to silence POSTN (Figure S4). si-POSTN-1 and si-POSTN-2 downregulated POSTN mRNA expression in CAF-S1/S2/S3/S4 cells (Figure 4b). Consistent with the cellular αLOX, POSTN knockdown decreased αLOX levels in sEVs isolated from the transfected CAF-S1/S2/S3/S4 cells (Figure 4c-d). These findings suggest that generation of αLOX in CAFs and their sEVs was dependent on POSTN.

CAF sEVs detect collagen I via surface integrin α2β1

Next, we analyzed the mechanisms by which CAF sEVs detect collagen. Integrin α2β1 is an important receptor involved in binding to collagen and activation of platelets. We hypothesized that integrin α2β1 may mediate the interactions between CAF sEVs and collagen (Figure 5a). The presence of integrin α2 and β1 and the absence of integrin α4 and α6 in CAF-S1/S2/S3/S4 sEVs were confirmed by western blotting (Figure 5b). Incubation of collagen I matrix with PKH-67-labeled CAF-S1/S2/S3/S4 sEVs with or without TC I-15, an inhibitor of integrin α2β1, showed that a large amount of sEVs adhered to the collagen matrix, and TC I-15 suppressed the adhesion of CAF-S1/S2/S3/S4 sEVs to collagen significantly (Figure 5c).

TEM was used to visualize collagen I with and without CAF sEV treatment for 12 h. Representative TEM images are shown in Figure 4d. In the absence of CAF-S2 sEVs, the collagen I matrix appeared as thin, short, and curved fibers, whereas the CAF-S2 sEV-treated group showed thick, long, and straight fibers. CAF-S2 sEVs physically adhered to thick collagen fibers, and the collagen crosslinking induced by CAF-S2 sEVs showed a diffuse pattern. Treatment with TC I-15 decreased the amount of thick and long fibers induced by CAF-S2 sEVs. Similar effects of CAF-S1/S3/S4 sEVs and TC I-15 on collagen crosslinking were observed (Figure S3). These findings indicate that CAF sEVs may detect collagen via integrin α2β1 and then directly induce collagen crosslinking catalyzed by CAF sEV-associated LOX.

Next, we examined whether the collagen crosslinking promoted by CAF sEVs could be blocked by interfering with the binding of sEVs to collagen. The collagen matrix was treated with CAF-S1/S2/S3/S4 sEVs with or without TC I-15 for 12 h. PBS was used as a negative control and glucose was used as a positive control. The levels of mature and immature collagen crosslinks were measured by ELISA (Figure 5e). The levels of PYD, DHLNL, and HLNL were significantly higher in the glucose and CAF-S1/S2/S3/S4 sEV groups than in the PBS group, and TC I-15 significantly inhibited CAF-S1/S2/S3/S4 sEV-induced upregulation of the mature collagen crosslink (PYD). The levels of immature collagen crosslinks (DHLNL and HLNL) were also lower in the CAF-S1/S2/S3/S4 sEV plus TC I-15 groups than in the CAF-S1/S2/S3/S4 sEV groups, although the difference was not consistently significant. These findings suggest that integrin α2β1 mediates the binding of CAF sEVs to collagen I.

CAF sEV-LOX causes EMT of OSCC spheroids *in vitro*

Collagen crosslinking causes ECM stiffness, which is a major regulator of EMT in cancer cells. We therefore examined the effect of CAF sEV-induced collagen crosslinking on OSCC cells *in vitro*. The experimental design is described in Figure 6a. UM-SCC6 cells were seeded in a collagen-Matrigel mixture and cultured for 2 days. The tumor cells were evenly distributed in the matrix on day 0 and formed spheroids on day 2. The formed UM-SCC6 spheroids were stimulated with CAF sEVs in the presence or absence of BAPN. PBS was used as the negative control. The morphology of the tumor spheroids was examined by staining cells with fluorescein phalloidin for F-actin and DAPI for nuclei. As shown in Figure 6b, UM-SCC6 spheroids were round and hardly invaded the surrounding matrix. By contrast, addition of CAF sEVs into the culture medium caused the extension of long processes and invasion of UM-SCC6 cells into the surrounding matrix. The spheroid areas in the CAF sEVs groups were significantly larger than those in the PBS group. BAPN treatment significantly reduced UM-SCC6 invasion induced by CAF sEVs. Immunofluorescence detection of the EMT biomarkers E-cadherin, N-cadherin, and vimentin in UM-SCC6 spheroids showed that CAF sEVs groups significantly decreased E-cadherin expression and significantly increased N-cadherin and vimentin expression compared with the PBS group (Figure 6b). BAPN rescued E-cadherin expression and downregulated N-cadherin and vimentin in UM-SCC6 spheroids, suggesting that CAF sEVs promote OSCC EMT in the 3D matrix via LOX. In addition, FAK^{Y397} expression in UM-SCC6 spheroids significantly increased in CAF sEV groups compared with the PBS group. BAPN significantly decreased FAK^{Y397} expression in UM-SCC6 spheroids (Figure 6b).

ELISA was used to measure the levels of mature and immature collagen crosslinks in the collagen-Matrigel mixture (Figure 6c). PYD, DHLNL, and HLNL levels increased significantly in the CAF-S2/S4 sEV groups compared with the PBS group, whereas BAPN treatment significantly decreased the levels of PYD, DHLNL, and HLNL induced by CAF-S2/S4. These findings suggest that CAF sEVs induce crosslinking of the collagen component in the collagen-Matrigel matrix and promote OSCC EMT.

CAF sEV-LOX causes EMT of OSCC xenografts *in vivo*

To determine the role of CAF sEV-LOX in the EMT of OSCC *in vivo*, nude mice were subcutaneously injected with UM-SCC6 cells. When the average diameter of xenografts reached approximately 5 mm at 2 weeks, CAF sEVs were injected into the peritumor region every 3 days with or without BAPN intraperitoneal injection every other day (Figure 7a). PBS was used as a control. The xenograft volume increased gradually in all groups (Figure S4a). At 6 weeks, the mice were sacrificed and xenografts were harvested (Figure S4b, Figure 7b). The xenograft weight was higher in the CAF sEV groups than in the sEV with BAPN groups, whereas the weight of the nude mice was comparable between the CAF sEV and CAF-S2/S4 sEV with BAPN groups (Figure S4c). The histopathological features of the xenografts were consistent with those of squamous cell carcinoma with low differentiation (Figure 7b). Xenografts in the CAF sEV groups tended to invade the covering skin and formed ulcerations (Figure 7b). BAPN significantly inhibited LOX expression in the xenografts (Figure 7c). E-cadherin expression was higher, whereas N-cadherin and vimentin were lower in the CAF-S2/S4 sEV plus BAPN xenografts than in the CAF-S2/S4 sEV groups (Figure 7c). These findings indicate that CAF sEV-LOX may modulate EMT of OSCC cells *in vivo*.

Clinical values of collagen crosslinking and sEV-LOX in OSCC patients

To investigate CAF-induced collagen crosslinking in OSCC patients, 40 OSCC cases and 14 normal controls were collected. Immunohistochemical staining identified higher expressions of FAP and α-SMA, biomarkers of CAFs, in the stroma of SACC cases than normal controls (Figure 8a). Picrosirius red staining showed that the amount of fibrillar collagen increased markedly in OSCC stroma compared with normal controls (Figure 8b). These findings suggest that CAFs promote collagen crosslinking in OSCC patients.

We tried to find the clinical values of plasmal EV-LOX in OSCC patients. Six OSCC cases and three healthy controls were examined. The expression of EV biomarkers, including CD63, CD9 and HSP 70, was confirmed in plasmal EVs of both OSCC patients and controls (Figure 8c). ELISA analysis revealed that plasmal EV-LOX showed higher expression in OSCC patients than normal controls (Figure 8d), suggesting that CAF-produced EV-LOX could be released into circulation.

Discussion

Collagen is the most abundant ECM scaffolding protein, and enhanced collagen crosslinking is associated with tumor progression [7, 37]. In this study, we demonstrated, for the first time, that sEVs derived from CAFs mediate collagen crosslinking directly. CAFs secrete αLOX-rich sEVs that detect collagen I via surface integrin α2β1 and subsequently induce collagen crosslinking, and collagen crosslinking promotes EMT in OSCC (Figure 9).

ProLOX and αLOX are generated by processing full-length LOX. BMP-1 catalyzes the extracellular proteolytic cleavage of proLOX to release αLOX and a propeptide [21, 38]. αLOX plays a critical role in the formation and repair of the ECM by catalyzing the crosslinking of collagen and elastin, which stabilizes these fibrous proteins [39, 40]. In this study, both proLOX and αLOX were detected in CAF cells, suggesting that at least a part of αLOX is generated in CAFs. The difference between the present results and those of previous studies might be due to the use of stromal cells in this study, whereas previous studies used various cancer cells. We demonstrated that CAFs express BMP-1, which cleaves proLOX, whereas most cancer cells do not express BMP-1 and need exogenous BMP-1 to catalyze the processing of proLOX secreted into the extracellular space. We showed that only αLOX, but not proLOX, was associated with CAF sEVs. We further demonstrated that αLOX interacts with POSTN, FN, and BMP-1 on the surface of CAF sEVs and is catalytically active, as indicated by its effect on collagen crosslinking. These findings suggest that CAF sEVs not only carry αLOX, but may also be responsible for the production of αLOX from proLOX catalyzed by the FN-POSTN-BMP-1 complex. The present findings provide new insight into the processing of proLOX into αLOX in stromal cells.

LOX is commonly known as a secreted protein, but not a membrane protein. It has been demonstrated that FN is captured on the surface of EVs by integrins or heparan sulfate proteoglycans [36, 41]. We demonstrated that αLOX is located on the surface of CAF sEVs by interacting with FN, POSTN and BMP-1. The functions of EV-associated FN include facilitating cellular uptake of EVs, promoting directional cancer cell movement, and inducing IL-1β expression by macrophages. We further demonstrate that EV-associated FN may serve as a reservoir for some soluble factors, which could not bind to EV directly.

EVs play important roles in cell-cell communication by delivering their cargo to recipient cells [35, 42-44]. However, limited information is available regarding the interaction between EVs and the ECM. A recent study identified several proteolytic proteins associated with EVs that may cleave ECM components [45]. Membrane type 1 matrix metalloproteinase (MT1-MMP) is an efficient ECM degrading enzyme. Functionally active MT1-MMP could be secreted from EVs and degrade type 1 collagen and gelatin [46]. Activated polymorphonuclear leukocytes secrete EVs with high levels of surface-bound neutrophil elastase. These EVs bind to the ECM via integrin MAC-1 and degrade collagen I via neutrophil elastase. When administered to mice, these EVs cause emphysema in animal models [47]. In this study, we found that CAFs released sEVs containing high levels of surface-bound αLOX. We showed that CAF sEVs bind to collagen I via integrin α2β1 and promote crosslinking of collagen directly via sEV-LOX. These findings expand the biological functions of EVs and highlight the important biological effects of these particles on both cells and the ECM.

LOX directly affects tumor progression by regulating collagen crosslinking and the stiffness of the ECM, which are factors that modulate cell invasion and tumor progression [7, 48]. LOX expression in patients with head and neck squamous cell carcinoma decreases metastasis-free and overall survival [49]. CAF-derived LOX in the liver metastatic niche of gastric cancer promotes tumor cell proliferation and outgrowth [50]. Stromal fibrosis accompanied by collagen crosslinking is common in OSCC. In this study, we demonstrated that CAF sEV-LOX promotes collagen crosslinking, thereby regulating the EMT of OSCC

cells *in vitro* and *in vivo*. These findings reveal a direct role of CAF sEV-associated LOX in collagen crosslinking and offer a new paradigm for understanding the positive association between CAFs in the stroma and increased invasive ability of OSCC. In addition, our study demonstrated that plasmal EV-LOX increased in OSCC patients. Further study is required to demonstrate whether these plasmal EV-LOX could trigger collagen crosslinking in distant organs.

Conclusions

In conclusion, CAF-released sEVs were rich in αLOX, which interacted with FN, POSTN, and BMP-1 on the surface of sEVs. Integrin α2β1 mediated the binding of CAF sEVs to collagen I, and αLOX triggered collagen crosslinking directly. Collagen crosslinking induced by CAF sEVs promoted the EMT of OSCC cells. These findings elucidate a critical mechanism underlying tumor ECM stiffness and reveal a novel role of sEVs in ECM remodeling and its effect on cancer cells.

Materials And Methods

Cell Culture

Four cases of fresh OSCC tissues were obtained from the First and Second Affiliated Hospitals, Dalian Medical University. CAFs were isolated from OSCC tissues and named CAF-S1, CAF-S2, CAF-S3 and CAF-S4, respectively [35]. Normal fibroblasts (NFs) were isolated from normal gingival tissues of a healthy adult during tooth extraction. CAFs and NFs were cultured in DMEM/F12 medium (Gibco, Grand Island, NY, USA). UM-SCC6 was a kind gift from Peking Union Medical University and cultured in DMEM/High Glucose medium (Hyclone, Logan, UT, USA). All cells were supplemented with 10% fetal bovine serum (FBS, ScienCell, Carlsbad, CA, USA), 100U/mL penicillin and 100U/mL streptomycin (Hyclone) at 37°C in a humidified 5% CO_2 incubator.

sEV separation and labeling

Bovine sEVs were depleted from FBS by ultracentrifugation. When cells reached 80% confluency, fresh DMEM/F12 medium with 2% sEV-depleted FBS was used to culture cells for another 72 h as conditioned medium (CM). Then, CM was collected and differentially centrifuged 500 *g* for 10 min, 2,500 *g* for 20 min, 12,000 *g* for 30 min and 100,000 *g* for 70 min. Then, the pellet was diluted in 20 mL phosphate buffer saline (PBS) and ultracentrifuged at 100,000 *g* for 70 min. For plasma EV separation, blood was collected into an EDTA-K2 anticoagulant tube, mixed immediately to avoid clotting, and sequentially centrifuged at 1,500 *g* and 2,400 *g* for 10 min at 4 °C. The supernatant was collected and diluted at ratio 1:1 with PBS followed by ultracentrifugation.

The protein concentration of sEVs was measured by BCA kit (Beyotime Biotechnology, shanghai, China). sEVs were labeled with PKH67 (Sigma-Aldrich, Louis, MO, USA) according to the company's instruction.

Labeled sEVs were re-separated by ultracentrifugation at 100,000 *g* for 70 min.

Transmission Electron microscopy (TEM)

sEVs in PBS were placed on a formvar carbon-coated grid for 20 min. The sample was negatively stained with 1% phosphotungstic acid solution for 5 min. For immunogold labeling, purified sEVs in PBS were placed on formvar carbon-coated grid for 20 min, washed with PBS twice and incubated 50 mM glycine to quench free aldehyde groups. After the grids were washed, they were

blocked using PBS containing 5% bovine serum albumin (BSA) for 1 h, and incubated with primary antibodies against CD63 (10 μg/mL, Abcam, Cambridgeshire, UK), CD9 (10 μg/mL, Abcam), LOX (10 μg/mL, Abcam) overnight at 4℃. Then, the samples were incubated with goat anti-rabbit IgG conjugated to 5 nm-colloidal gold particles (Invitrogen). Then the grid was washed with PBS contained 0.1%BSA and fixed with 2.5% glutaraldehyde for 15 min then thoroughly washed with deionized water. Samples were counterstained with phosphato-tungstic acid for 5 min. Images were taken using a transmission electron microscope (JEM-2000EX*, Japan Electronics, Japan).

Western Blot analysis

Cells or sEVs were lysed by RIPA buffer (Millipore Corporation, Billerica, MA, USA) supplemented with PMSF (100 mM, Solarbio, Beijing, China) and cocktail protease inhibitors (Sigma-Aldrich) at 4℃ for 15 min. Protein concentration was determined by BCA kit (Beyotime Biotechnology). Equal amount of proteins was separated by sodium dodecyl sulfate-polyacrylamide gel. Proteins on gel were transferred onto a nitrocellulose membrane (Millipore Corporation). Then, the membrane was blocked with 5% fat-free milk for 2 h followed by primary antibodies incubation at 4℃ overnight. Primary antibodies included CD63 (1:500; Abcam), CD9 (1:500; Abcam), HSP70 (1:500; Abcam), CALNEXIN (1:500; Proteintech, Wuhan, China), LOX (1:600; Abcam), POSTN (1:500; Abcam), BMP-1 (1:300; Bioss, Beijing, China), FN (1:500; Abcam), integrin α2 (1:500, Abcam), integrin α4 (1:500; Abcam), integrin β1 (1:500; Abcam), vimentin (1:1000; Abcam), FSP-1(1:1000; Abcam), FAP (1:500; Abcam), α-SMA (1:1000; Proteintech, Wuhan, China), and GAPDH (1:3000; Proteintech). After the membrane incubation with horseradish peroxidase (HRP)-labelled IgG (H+L) as secondary antibody (1:3000; Proteintech) for 1 h. Protein bands were detected with Enhanced chemiluminescence detection system (ChemiDoc XRS, Bio-Rad).

RNA isolation and quantitative reverse transcription-polymerase chain reaction (qRT-PCR)

Total RNA was extracted using Trizol Reagent (Invitrogen). The PrimerScript RT reagent Kit (TaKaRa, Dalian, China) was used for reverse transcription. Quantitative real-time PCR reaction was performed with

SYBR Premix Ex Taq reagent kit (TaKaRa) using Thermal Cycler Dice Real Time System (TaKaRa). GAPDH was used as an internal control. The primers for POSTN and GAPDH were purchased from TaKaRa. Primer sequences were as following: POSTN (forward): 5'-CCA TCA CAT CGG ACA TAT TGG A-3', (reverse): 5'-TGC TCC TCC CAT AAT AGA CTC A-3'; GAPDH (forward): 5'-GTG AAG GTC GGA GTC AAC G-3', (reverse): 5'-TGA GGT CAA TGA AGG GGT C-3'. Each experiment was repeated at least three times.

Immunoprecipitation (IP)

Protein A/G plus-magnetic beads (SelleckChem, Shanghai, China) was incubated with anti-POSTN antibody (Santa Cruz Biotechnology) under rotation for 15 min, followed by incubating with the protein extract from cells or sEVs for 15 min. The immunoprecipitated proteins were washed and resuspended in loading buffer, denatured and submitted to western blot analysis.

Enzyme-linked immunosorbent assay (ELISA)

To detect LOX or POSTN in sEVs, ELISA kits was purchased (LOX: Elabscience #H0174c; POSTN: Elabscience #H2452c). sEVs separated from CM were prepared for the serial dilution were added into each well (100 μL/well). Plasmal sEVs (100 μg) or sEV-excluded plasma (100 μg) were added into each well (100 μL/well). After 90 min, biotinylated LOX or POSTN antibody was added into each well and incubated at 37℃ for 1h. Then, horseradish peroxidase-conjugated streptavidin (100 μL) was added and incubated at 37℃ for 30 min followed by incubation with 3,3',5,5'-tetramethylbenzidine substrate reagent at 37℃ for 15 min. After adding 50 μL of stop solution to each well, the absorbance at 450 nm was measured with a microplate reader (ThermoFisher scientific, Waltham, MA, USA). To block the sEV surface LOX or POSTN, LOX or POSTN blocking antibodies (10 μg/mL) in 100 μL PBS were used to incubate with sEVs at 4℃ overnight, washed with PBS (20 mL), and pelleted by ultracentrifugation to remove non-bound antibodies. Each experiment was repeated at least three times.

siRNA transfection

Two POSTN gene-specific short interfering RNA (siPOSTN-1: 5' - CCC AUG GAG AGC CAA UUA UTT-3' and siPOSTN-2: 5'-CUC UGA CAU CAU GAC AAC AAA UTT-3') and a negative control siRNA (si-NC: 5'-UUC UCC GAA CGU GUC ACG UTT-3') were synthesized by Genepharma (Shanghai, China). They were transfected into cells with Lipofectamine™ 2000 reagent (Invitrogen) according to manufacturer's instructions. After 48 h, total RNA and protein were isolated from transfected cells. sEVs were separated from the CM of transfected cells.

sEV treatment of human NFs

To assess the interactions of CAF sEVs with stromal cells and ECM, NFs (1×10^5 cells/well) labeled with CellTracker Red CMTPX Dye (Invitrogen) were cultured in a 12-well plate for 12 h or 72 h. Then, PKH67-labeled sEVs (20 μg/well) were added into each well and incubated for 12 h. After washing with PBS, NFs were fixed with 4% paraformaldehyde for 15 min. Nuclei were counterstained with DAPI (Thermo Fisher Scientific). Images were recorded by an inverted microscope (Olympus IX71, Tokyo, Japan).

To test collagen cross-linking, NFs (1×10^5 cells/well) were seeded in a 6-well plate and cultured for 72 h. Purified sEVs (100 μg/well) were added into each well and incubated for 12 h. Fox LOX inhibition, sEVs (100 μg) were pre-incubated with β-amino propionitrile (BAPN, 200 μM) and the LOX-blocking antibody (10 μg/mL) at 4℃ overnight. The immature crosslinks, DHLNL and HLNL, and a mature crosslink, PYD, were quantified by ELISA assay. ELISA kits (DHLNL: Jonln #JL47954, HLNL: Jonln #JL47940, PYD: Jonln #JL19698) were purchased from Shanghai JONLN Reagent Co., Ltd., China. The absorbance at 450 nm was measured using a microplate reader (ThermoFisher scientific).

sEV treatment of human collagen matrix

To confirm sEVs bond to collagen matrix, type I collagen (3 mg/mL, Corning, Bedford, MA, USA) was mixed with Matrigel (Corning) at ratio 2:1 and added to a 48-well plate and incubated for 30 min at 37℃. Then PKH67-labeled sEVs (20 μg/well) were added into the collagen I-containing wells and incubated at 37℃ for 12 h. To inhibit integrin α2β1-mediated collagen binding, sEVs were pre-incubated with 2 μM TCI-15 (TOCRIS, Oxfordshire, UK) at 37℃ for 1 h. After washing with PBS, images were recorded by an inverted fluorescent microscope (Olympus IX71).

To visualize sEV-stimulated collagen crosslinking, collagen I (5 μg) was mixed with 20 μg sEVs and incubated for 12 h at 4℃. PBS was used as a control. The samples were placed on a formvar carbon-coated grid for 20 min, then negatively stained with 1% phosphotungstic acid solution for 5 min. Any excess of stain was wicked away and grid was air-dried at room temperature. Images were recorded using a transmission electron microscope (JEM-2000EX*).

To detect collagen crosslinks, sEVs (100 μg) mixed with collagen I (Corning) were added into a 24-well plate and incubated for 12 h. PYD, DHLNL, and HLNL were quantified by ELISA assay.

Tumor spheroid assay *in vitro*

Collagen I (2 mg/mL) was mixed with Matrigel in the ratio 1: 2 by volume. A 96-well plate was pre-coated with the collagen I-Matrigel mixture (30 μL/well). UM-SCC6 cells were suspended in the collagen I-Matrigel mixture and added to the precoated 96-well plate (3.75×10^4 cells in 75 μL/well). After the mixture gelled, DMEM/High Glucose medium (100 μL/well) was added into each well. After 2 days, tumor cells formed spheroids in the wells and CAF sEVs (100 μg) were added into each well with or without BAPN (200 μM). PBS was used as a control. After another 2 days, tumor spheroids were fixed with

4% paraformaldehyde for 15 min and permeabilized with PBS containing 0.025% Triton X-100. Samples were blocked using normal goat serum containing 5% BSA for 2 h at room temperature, then incubated with primary antibodies, including E-cadherin (1:100, Abcam), N-cadherin (1:100, Abcam), vimentin (1:100, Abcam) and FAK^{Y397} (1:100, Abcam)

overnight at 4℃. Next day the samples were incubated with DyLight 549-conjugated secondary antibody (1:200, Abbkine, Wuhan, China) and nuclei were counterstained with DAPI (1:3000, Thermo Fisher Scientific). TRITC Phalloidin (1:200, YEASEN, Shanghai, China) staining was performed to observed cellular morphologies. Images were recorded using a Nikon confocal microscope (Nikon A1R). UM-SCC6 spheroid area and expression areas of E-cadherin, N-cadherin, Vimentin and FAK^{Y397} were quantified with Image Pro Plus 6.0 using 5 random high-power fields of each well.

To detect collagen crosslinks, collagen I-Matrigel mixture (75 μL/well) in a 96-well plate was treated by CAF sEVs (100 μg/well) with and without BAPN (200 μM) for 12 h. Then, the levels of PYD, DHLNL, and HLNL in the mixture were quantified by ELISA assay.

Animal models

UM-SCC6 cells (2×10^6 cells /mouse) were injected into the subcutaneous space of nude mice aged 6 weeks old (about 18 g, female). After 2 weeks, the average diameter of subcutaneous xenografts was around 5 mm. CAF sEVs (100 μg/mouse) were injected into the peritumor region every 3 days. BAPN (100 mg/kg) was injected intraperitoneally every other day. PBS was used as a control. Mice were weighed every 3 days. Xenografts were measured using calipers every week and the volumes were calculated by the formula: $(\text{width})^2 \times \text{length}/2$. When most xenografts reached 1000 mm^3 at week 6, mice were sacrificed. Xenografts were harvested and fixed in 10% formalin buffer for 24 h, embedded in paraffin. Hematoxylin and eosin (HE) staining was performed to confirm the histological features of these xenografts. Immunofluorescent staining was performed to assess EMT. Primary antibodies included LOX (1:200, Abcam), E-cadherin (1:100, Abcam), N-cadherin (1:100, Abcam), vimentin (1:100, Abcam). All animal experiments were strictly performed in accordance with animal care guidelines approved by the Animal care and Use Committee of Dalian Medical University.

Statistical analyses

GraphPad Prism 7.0 (Graphpad Software Inc.) and Image Pro Plus 6.0 was used for statistical analyses. Unpaired Student's t-tests was performed for comparisons between all of the data. Error bars shown in graphical data represent the mean ± SD. Statistical significance was defined as $p< 0.05$. Each experiment was repeated at least three times.

Abbreviations

CAFs: Carcinoma-associated fibroblasts; ECM: Extracellular matrix; LOX: Lysyl oxidase; EVs: Extracellular vesicles; sEVs: Small extracellular vesicles; OSCC: Oral squamous cell carcinoma; EMT: Epithelial-mesenchymal transition; DHLNL: dihydroxylysino-norleucine; HLNL: hydroxylysino-norleucine; PYD: pyridinoline; αLOX: Active LOX; BMP-1: Bone morphogenetic protein-1; POSTN: Periostin; FN: fibronectin; BAPN: β-amino propionitrile; NFs: Normal fibroblasts; FBS: Fetal bovine serum; BSA: bovine serum albumin; CM: Conditioned medium; PBS: Phosphate buffer saline; MT1-MMP: Membrane type 1 matrix metalloproteinase; TEM: Transmission Electron microscopy; qRT-PCR: Quantitative reverse transcription-polymerase chain reaction; ELISA: Enzyme-linked immunosorbent assay; HE: Hematoxylin and eosin; IP: Immunoprecipitation.

Declarations

Ethics approval and consent to participate

The use of human samples was approved by the Ethics Committee of Dalian Medical University. Animal tests were conducted in compliance with the guidelines issued by the Ethical Committee of Dalian Medical University.

Consent for publication

All authors of this article have directly participated in the planning and drafting and all authors listed have read and approved the final version including details and images. The written informed consent for the publication has been obtained from all the authors.

Availability of data and materials

All the data generated or analyzed during this study are included in this published article and its supplementary files. The datasets and materials in the current study available from the corresponding author on reasonable request.

Competing interests

The authors report no conflict of interest.

Funding

National Natural Science Foundation of China (No: 82073001 and 82103423), Dalian Science and Technology Innovation Project (2020JJ26SN053), Scientific Research Foundation for the Introduction of Talent in Shanghai Stomatological Hospital (SSDC-2021-RC01).

Authors' contributions

TJL and YHL designed this study. DYQ, FYZ, and BS provided clinical samples. XL, JL, XSY, XJL, and JK participated in the experiments. XL analyzed the data. TJL and YHL wrote the main manuscript text. All

authors read and approved the final manuscript.

Acknowledgements

Not applicable.

Author details

[1]Department of Oral Pathology, Shanghai Stomatological Hospital & School of Stomatology, Fudan University, Tianjin Road No.2, Huangpu District, Shanghai 200001, China. [2]Shanghai Key Laboratory of Craniomaxillofacial Development and Diseases, Fudan University, Tianjin Road No.2, Huangpu District, Shanghai 200001, China. [3]School of Stomatology, Dalian Medical University, West Section No.9, South Road of Lvshun, Dalian 116044, China. [4]Department of Orthodontics, Shanghai Stomatological Hospital & School of Stomatology, Fudan University, Tianjin Road No.2, Huangpu District, Shanghai 200001, China. [5]Department of Biochemistry and Molecular Biology, Liaoning Provincial Core Lab of Glycobiology and Glycoengineering, Dalian Medical University, West Section No.9, South Road of Lvshun, Dalian 116044, China. [6] Department of Oral Surgery, the First Affiliated Hospital of Dalian Medical University, No.222 Zhongshan Road, Dalian 116023, China. [7]Department of Oral Surgery, the Second Affiliated Hospital of Dalian Medical University, No.467 Zhongshan Road, Dalian 116023, China.

References

1. Gascard P, Tlsty TD. Carcinoma-associated fibroblasts: orchestrating the composition of malignancy. Genes Dev. 2016;30(9):1002-19.
2. Quante M, Tu SP, Tomita H, Gonda T, Wang SSW, Takashi S, et al. Bone marrow-derived myofibroblasts contribute to the mesenchymal stem cell niche and promote tumor growth. Cancer Cell. 2011;19(2):257-72.
3. Tang X, Hou Y, Yang G, Wang X, Tang S, Du YE, et al. Stromal miR-200s contribute to breast cancer cell invasion through CAF activation and ECM remodeling. Cell Death Differ. 2016;23(1):132-45.
4. van der Rest M, Garrone R. Collagen family of proteins. FASEB J. 1991;5(13):2814-23.
5. Bornstein P, Sage EH. Matricellular proteins: extracellular modulators of cell function. Curr Opin Cell Biol. 2002;14(5):608-16.
6. Georges PC, Hui JJ, Gombos Z, McCormick ME, Wang AY, Uemura M, et al. Increased stiffness of the rat liver precedes matrix deposition: implications for fibrosis. Am J Physiol Gastronintest Liver Physiol. 2007;293(6):G1147-54.
7. Levental KR, Yu H, Kass L, Lakins JN, Egeblad M, Erler JT, et al. Matrix crosslinking forces tumor progression by enhancing integrin signaling. Cell. 2009;139(5):891-906.
8. Yang J, Mani SA, Donaher JL, Ramaswamy S, Itzykson RA, Come C, et al. Twist, a master regulator of morphogenesis, plays an essential role in tumor metastasis. Cell. 117(7):927-39.

9. Eckert MA, Lwin TM, Chang AT, Kim J, Danis E, Ohno-Machado L, et al. Twist1-induced invadopodia formation promotes tumor metastasis. Cancer Cell. 2011;19(3):372-86.
10. Wei SC, Fattet L, Tsai JH, Guo Y, Pai VH, Majeski HE, et al. Matrix stiffness drives epithelial-mesenchymal transition and tumour metastasis through a TWIST1-G3BP2 mechanotransduction pathway. Nat Cell Biol. 2015;17(5):678-88.
11. Barriga EH, Franze K, Charras G, Mayor R. Tissue stiffening coordinates morphogenesis by triggering collective cell migration in vivo. Nature. 2018;554(7693):523-27.
12. Fattet L, Jung HY, Matsumoto MW, Aubol BE, Kumar A, Adams JA, et al. Matrix Rigidity Controls Epithelial-Mesenchymal Plasticity and Tumor Metastasis via a Mechanoresponsive EPHA2/LYN Complex. Dev Cell. 2020;54(3):302-316.e7.
13. Myllyharju J, Kivirikko KI. Collagens, modifying enzymes and their mutations in humans, flies and worms. Trends Genet. 2004;20(1):33-43.
14. Yamauchi M, Taga Y, Hattori S, Shiiba M, Terajima M. Analysis of collagen and elastin cross-links. Methods in Cell Biol. 2018;143:115-32.
15. Chitty JL, Setargew YFI, Cox TR. Targeting the lysyl oxidases in tumour desmoplasia. Biochem Soc Trans. 2019;47(6):1661-78.
16. Pankova D, Chen Y, Terajima M, Schliekelman MJ, Baird BN, Fahrenholtz M, et al. Cancer-Associated Fibroblasts Induce a Collagen Cross-link Switch in Tumor Stroma. Mol Cancer Res. 2016;14(3):287-95.
17. Yamauchi M, Terajima M, Shiiba M. Lysine Hydroxylation and Cross-Linking of Collagen. Methods Mol Biol. 2019;1934:309-24.
18. Trackman PC, Bedell-Hogan D, Tang J, Kagan HM. Post-translational glycosylation and proteolytic processing of a lysyl oxidase precursor. J Biol Chem. 1992;267(12):8666-71.
19. Grimsby JL, Lucero HA, Trackman PC, Ravid K, Kagan HM. Role of lysyl oxidase propeptide in secretion and enzyme activity. J Cell Biochem. 2010;111(5):1231-43.
20. Panchenko MV, Stetler-Stevenson WG, Trubetskoy OV, Gacheru SN, Kagan HM. Metalloproteinase activity secreted by fibrogenic cells in the processing of prolysyl oxidase. Potential role of procollagen C-proteinase. J Biol Chem. 1996;271(12):7113-9.
21. Uzel MI, Scott IC, Babakhanlou-Chase H, Palamakumbura AH, Pappano WN, Hong HH, et al. Multiple bone morphogenetic protein 1-related mammalian metalloproteinases process pro-lysyl oxidase at the correct physiological site and control lysyl oxidase activation in mouse embryo fibroblast cultures. J Biol Chem. 2001;276(25):22537-43.
22. Norris RA, Damon B, Mironov V, Kasyanov V, Ramamurthi A, Moreno-Rodriguez R, et al. Periostin regulates collagen fibrillogenesis and the biomechanical properties of connective tissues. J Cell Biochem. 2007;101(3):695-711.
23. Garnero P. The contribution of collagen crosslinks to bone strength. Bonekey Rep. 2012;1:182.

24. Maruhashi T, Kii I, Saito M, Kudo A. Interaction between periostin and BMP-1 promotes proteolytic activation of lysyl oxidase. J Biol Chem. 2010;285(17):13294-303.
25. Valadi H, Ekström K, Bossios A, Sjöstrand M, Lee JJ, Lötvall JO. Exosome-mediated transfer of mRNAs and microRNAs is a novel mechanism of genetic exchange between cells. Nat Cell Biol. 2007;9(6):654-9.
26. Skog J, Wurdinger T, van Rijn S, Meijer DH, Gainche L, Sena-Esteves M, et al. Glioblastoma microvesicles transport RNA and proteins that promote tumour growth and provide diagnostic biomarkers. Nat Cell Biol. 2008;10(12):1470-6.
27. Mulcahy LA, Pink R C, Carter DR. Routes and mechanisms of extracellular vesicle uptake. J Extracell Vesicles. 2014;3.doi: 10.3402/jev.v3.24641.
28. van Niel G, D'Angelo G, Raposo G. Shedding light on the cell biology of extracellular vesicles. Nat Rev Mol Cell Biol. 2018;19(4):213-28.
29. Pan BT, Teng K, Wu C, Adam M, Johnstone RM. Electron microscopic evidence for externalization of the transferrin receptor in vesicular form in sheep reticulocytes. J Cell Biol. 1985;101(3):942-8.
30. Raposo G, Stoorvogel W. Extracellular vesicles: exosomes, microvesicles, and friends. J Cell Biol. 2013;200(4):373-83.
31. Mathieu M, Martin-Jaular L, Lavieu G, Théry C. Specificities of secretion and uptake of exosomes and other extracellular vesicles for cell-to-cell communication. Nat Cell Biol. 2019;21(1):9-17.
32. Thery C, Witwer KW, Aikawa E, Alcaraz MJ, Anderson JD, Andriantsitohaina R, et al. Minimal information for studies of extracellular vesicles 2018 (MISEV2018): a position statement of the International Society for Extracellular Vesicles and update of the MISEV2014 guidelines." J Extracell Vesicles. 2018;7(1):1535750.
33. Becker A, Thakur BK, Weiss JM, Kim HS, Peinado H, Lyden D. Extracellular Vesicles in Cancer: Cell-to-Cell Mediators of Metastasis. Cancer Cell. 2016;30(6):836-48.
34. Kalluri R, LeBleu VS. The biology, function, and biomedical applications of exosomes. Science. 2020;367(6478): eaau6977.
35. Li J, Liu X, Zang S, Zhou J, Zhang F, Sun B, et al. Small extracellular vesicle-bound vascular endothelial growth factor secreted by carcinoma-associated fibroblasts promotes angiogenesis in a bevacizumab-resistant manner. Cancer Lett. 2020;492:71-83.
36. Purushothaman A, Bandari SK, Liu J, Mobley JA, Brown EE, Sanderson RD. Fibronectin on the surface of Myeloma Cell-derived Exosomes Mediates Exosome-Cell Interactions. J Biol Chem. 2016;291(4):1652-63.
37. Mouw JK, Ou G, Weaver VM. Extracellular matrix assembly: a multiscale deconstruction. Nat Rev Mol Cell Biol. 2014;15(12):771-785.
38. Hopkins DR, Keles S, Greenspan DS. The bone morphogenetic protein 1/Tolloid-like metalloproteinases. Matrix Biol. 2007;26(7):508-23.

39. Csiszar K. Lysyl oxidases: a novel multifunctional amine oxidase family. Prog Nucleic Acid Res Mol Biol. 2001;70:1-32.
40. Kagan HM, Li W. Lysyl oxidase: properties, specificity, and biological roles inside and outside of the cell. J Cell Biochem. 2003;88(4):660-72.
41. Sung BH, Ketova T, Hoshino D, Zijlstra A, Weaver AM. Directional cell movement through tissues is controlled by exosome secretion. Nat Commun. 2015;6:7164.
42. Chen G, Huang AC, Zhang W, Zhang G, Wu M, Xu W, et al. Exosomal PD-L1 contributes to immunosuppression and is associated with anti-PD-1 response. Nature. 2018;560(7718):382-86.
43. Tan E, Asada HH, Ge R. Extracellular vesicle-carried Jagged-1 inhibits HUVEC sprouting in a 3D microenvironment. Angiogenesis. 2018;21(3):571-80.
44. Kong J, Tian H, Zhang F, Zhang Z, Li J, Liu X, et al. Extracellular vesicles of carcinoma-associated fibroblasts creates a pre-metastatic niche in the lung through activating fibroblasts. Mol Cancer. 2019;18(1):175.
45. Sanderson RD, Bandari SK, Vlodavsky I. Proteases and glycosidases on the surface of exosomes: Newly discovered mechanisms for extracellular remodeling. Matrix Biol. 2019;75-76:160-169.
46. Hakulinen J, Sankkila L, Sugiyama N, Lehti K, Keski-Oja J. Secretion of active membrane type 1 matrix metalloproteinase (MMP-14) into extracellular space in microvesicular exosomes. J Cell Biochem. 2008;105(5):1211-1218.
47. Genschmer KR, Russell DW, Lal C, Szul T, Bratcher PE, Noerager BD, et al. Activated PMN Exosomes: Pathogenic Entities Causing Matrix Destruction and Disease in the Lung. Cell. 2019;176(1-2):113-126.e15.
48. Chaudhuri O, Koshy ST, Branco da Cunha C, Shin JW, Verbeke CS, Allison KH, et al. Extracellular matrix stiffness and composition jointly regulate the induction of malignant phenotypes in mammary epithelium. Nat Mater. 2014;13(10):970-78.
49. Chen Y, Shi G, Xia W, Kong C, Zhao S, Gaw AF, et al. Identification of hypoxia-regulated proteins in head and neck cancer by proteomic and tissue array profiling. Cancer Res. 2004; 64(20):7302-10.
50. Li Q, Zhu CC, Ni B, Zhang ZZ, Jiang SH, Hu LP, et al. Lysyl oxidase promotes liver metastasis of gastric cancer via facilitating the reciprocal interactions between tumor cells and cancer associated fibroblasts. EBioMedicine. 2019;49:157-171.

Figures

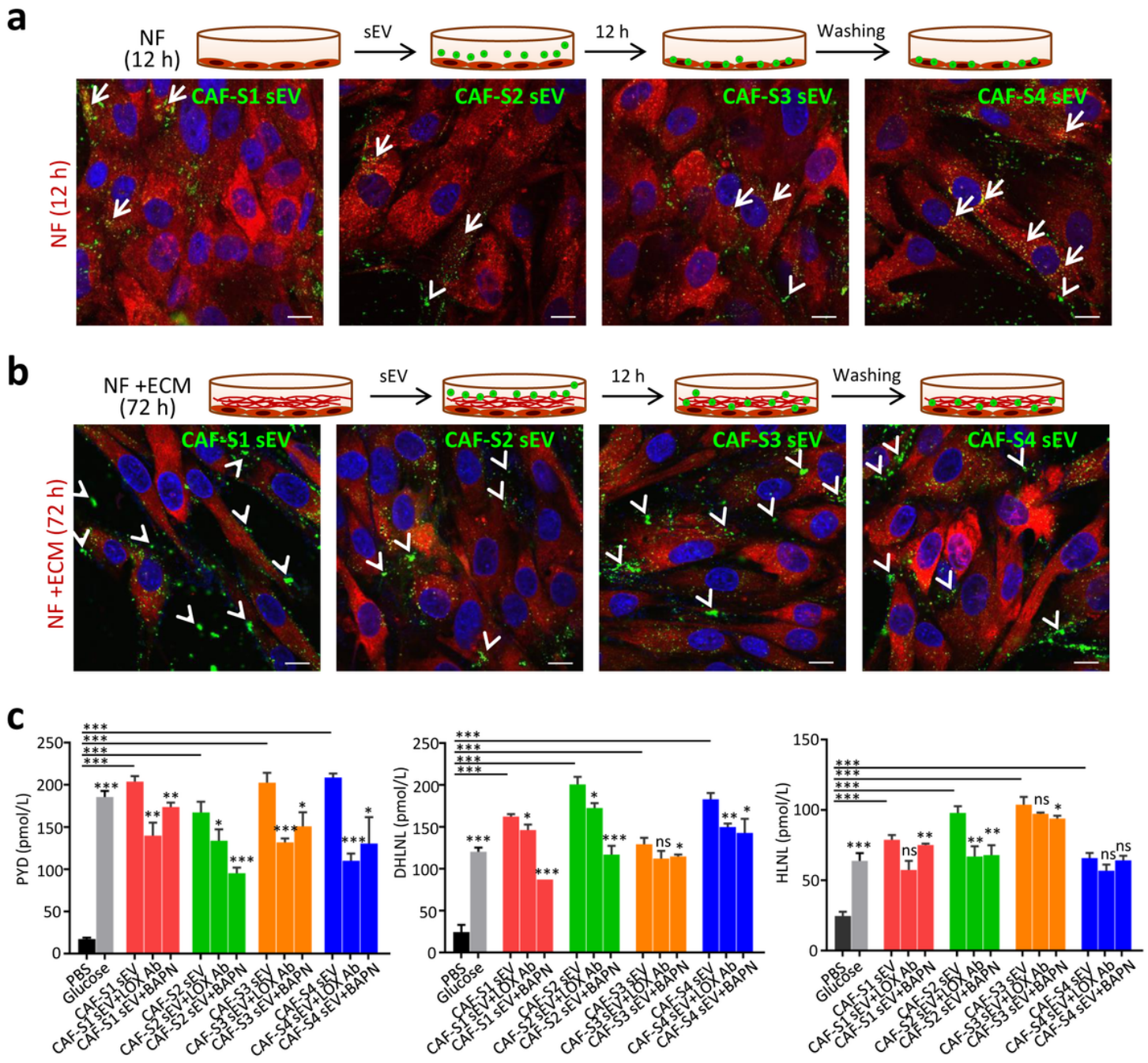

Figure 1

Collagen crosslinking triggered by CAF sEVs. (a) Internalization of CAF-S1/S2/S3/S4 sEVs (green) by cells. Normal fibroblasts (NFs) were cultured for 12 h. (b) Adhesion of CAF-S1/S2/S3/S4 sEVs (green) to ECM. Normal fibroblasts (red) were cultured for 72 h. (c) ELISA assay of PYD, DHLNL, and HLNL. NFs were cultured for 72 h, then treated with CAF-S1/S2/S3/S4 sEVs with or without anti-LOX antibody or BAPN. PBS was used as a negative control and glucose was used as a positive control. Scale bar = 10 μm. *$p < 0.05$, **$p < 0.01$ and ***$p < 0.001$.

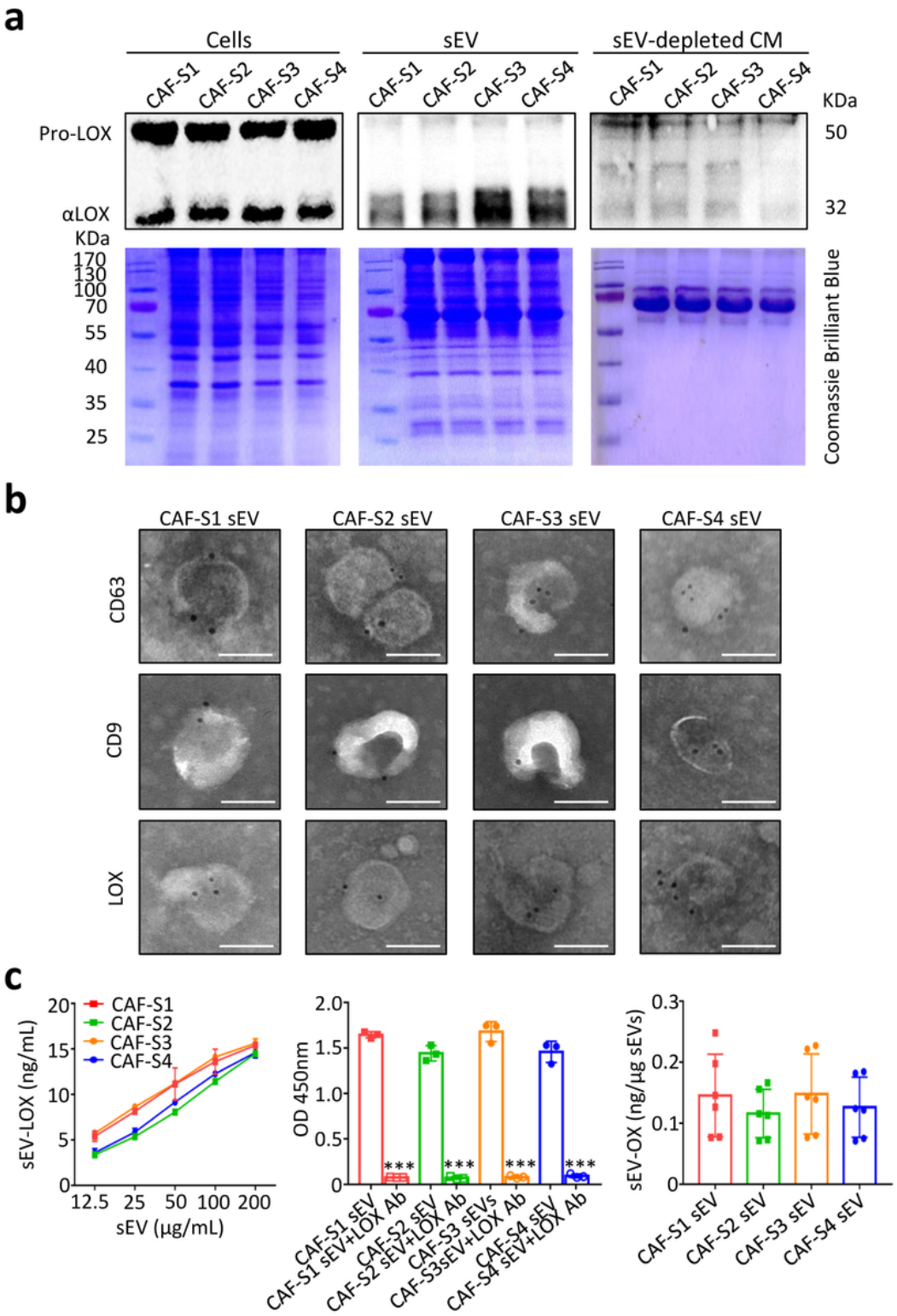

Figure 2

LOX expression patterns in CAF sEVs. (a) Western blot analysis of proLOX and αLOX expression in CAF-S1/S2/S3/S4 cells, sEVs, and sEV-depleted CM. (b) Immunogold labeling of CD63, CD9 and LOX on CAF-S1/S2/S3/S4 sEVs. Scale bar = 100 nm. (c) ELISA examination of LOX in CAF-S1/S2/S3/S4 sEVs.

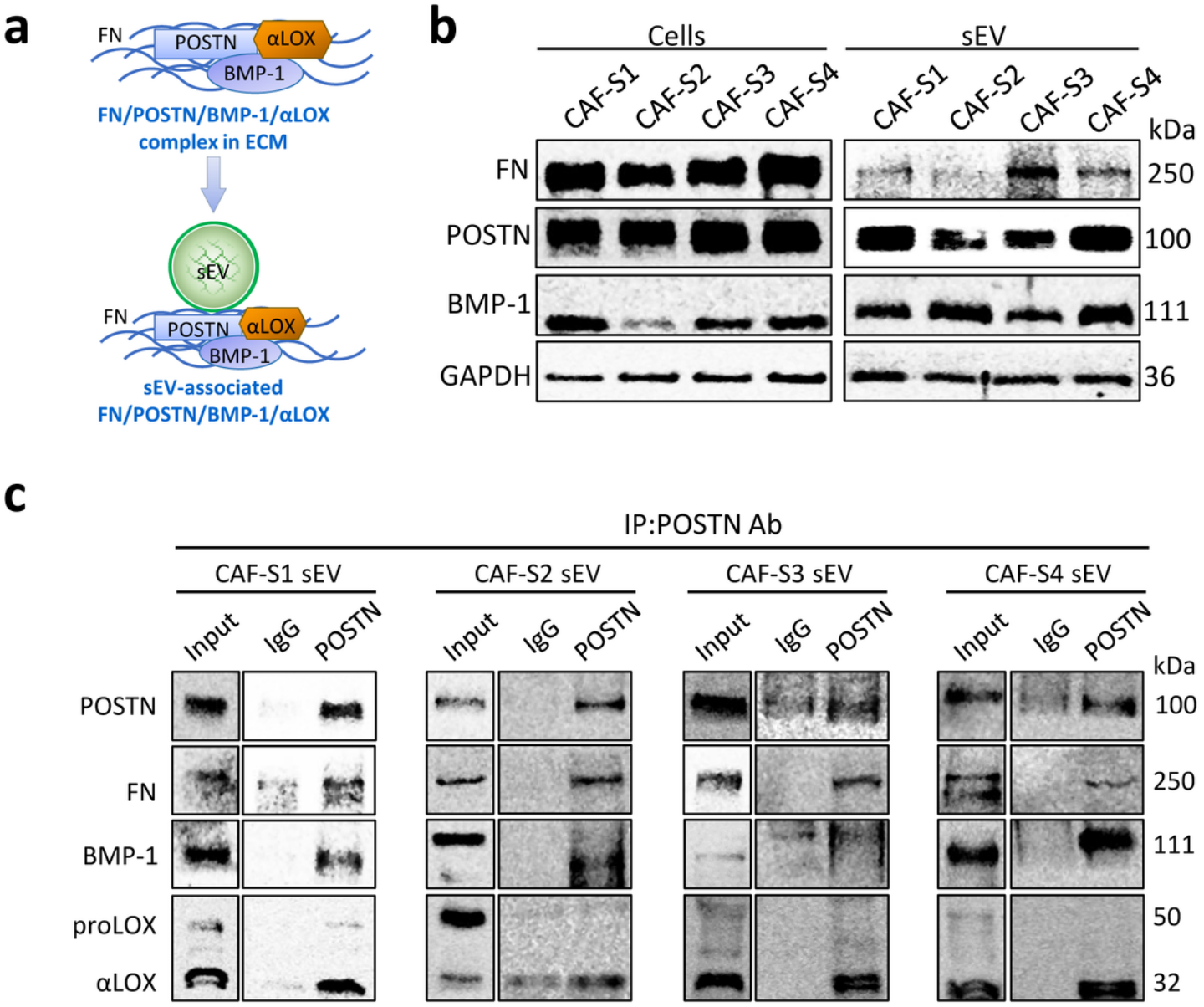

Figure 3

FN/POSTN/BMP-1/αLOX complex associated with CAF sEVs. (a) Schematic of FN/POSTN/BMP-1/αLOX complex associated with sEVs. (b) Western blot analysis of the expression of POSTN, FN, and BMP-1 in CAF-S1/S2/S3/S4 and their sEVs. (c) IP examination of POSTN interaction with FN, BMP-1 and αLOX in CAF-S1/S2/S3/S4 sEVs.

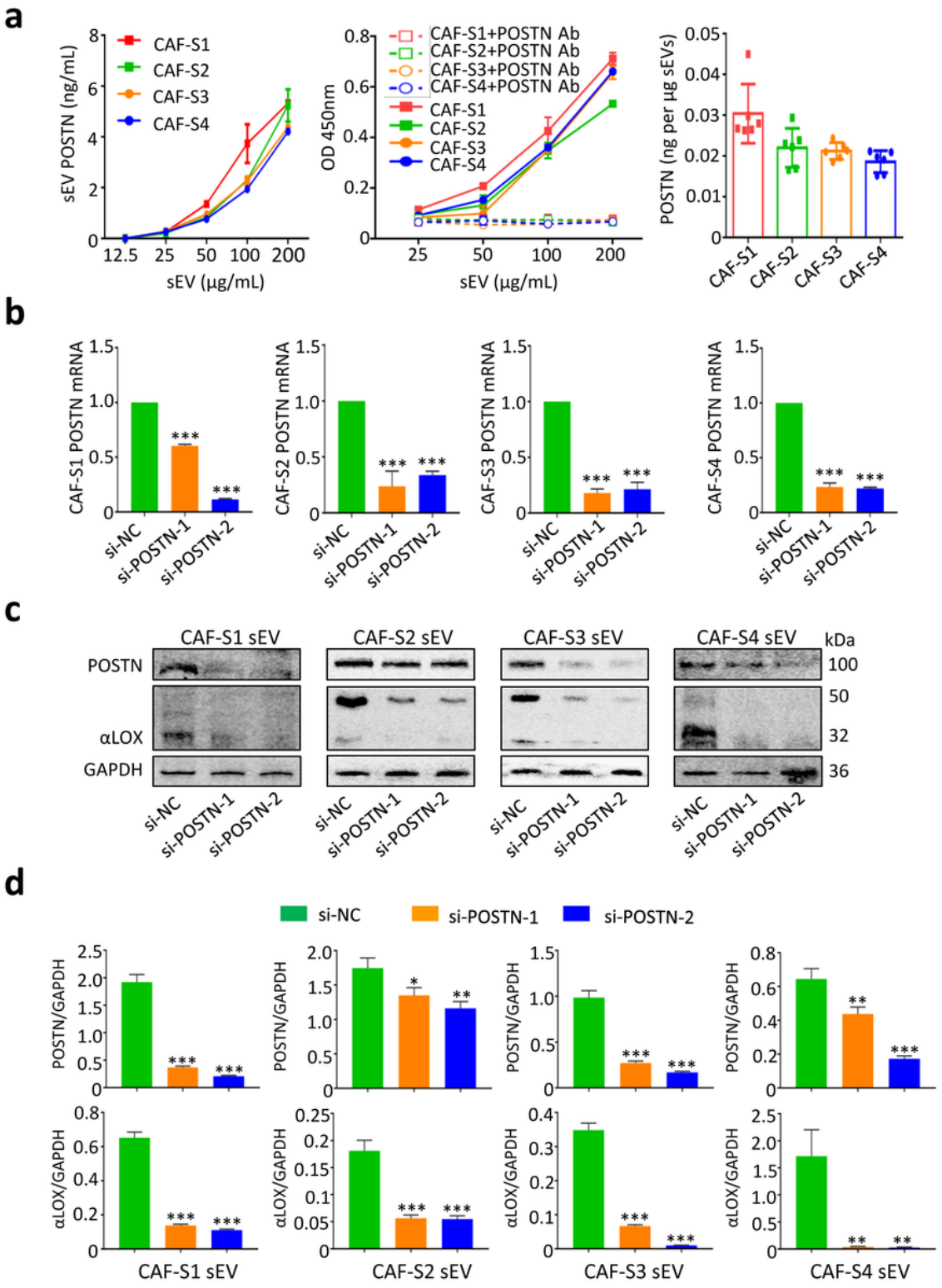

Figure 4

Regulation of αLOX by POSTN in CAF and their sEVs. (a) ELISA examination of POSTN in CAF-S1/S2/S3/S4 sEVs. (b) qRT-PCR analysis confirmed the downregulation of POSTN mRNA expression in CAF-S1/S2/S3/S4 induced by transfection with si-POSTN-1 or si-POSTN-2 compared with si-NC. (c) Western blot analysis demonstrated that transfection with si-POSTN-1 or si-POSTN-2 downregulated the expression of POSTN and αLOX in CAF-S1/S2/S3/S4 sEVs compared with that in cells transfected with

si-NC. (d) Quantitative analysis of POSTN and αLOX protein expression in CAF-S1/S2/S3/S4 sEVs with POSTN downregulation. *$p < 0.05$, **$p < 0.01$ and ***$p < 0.001$.

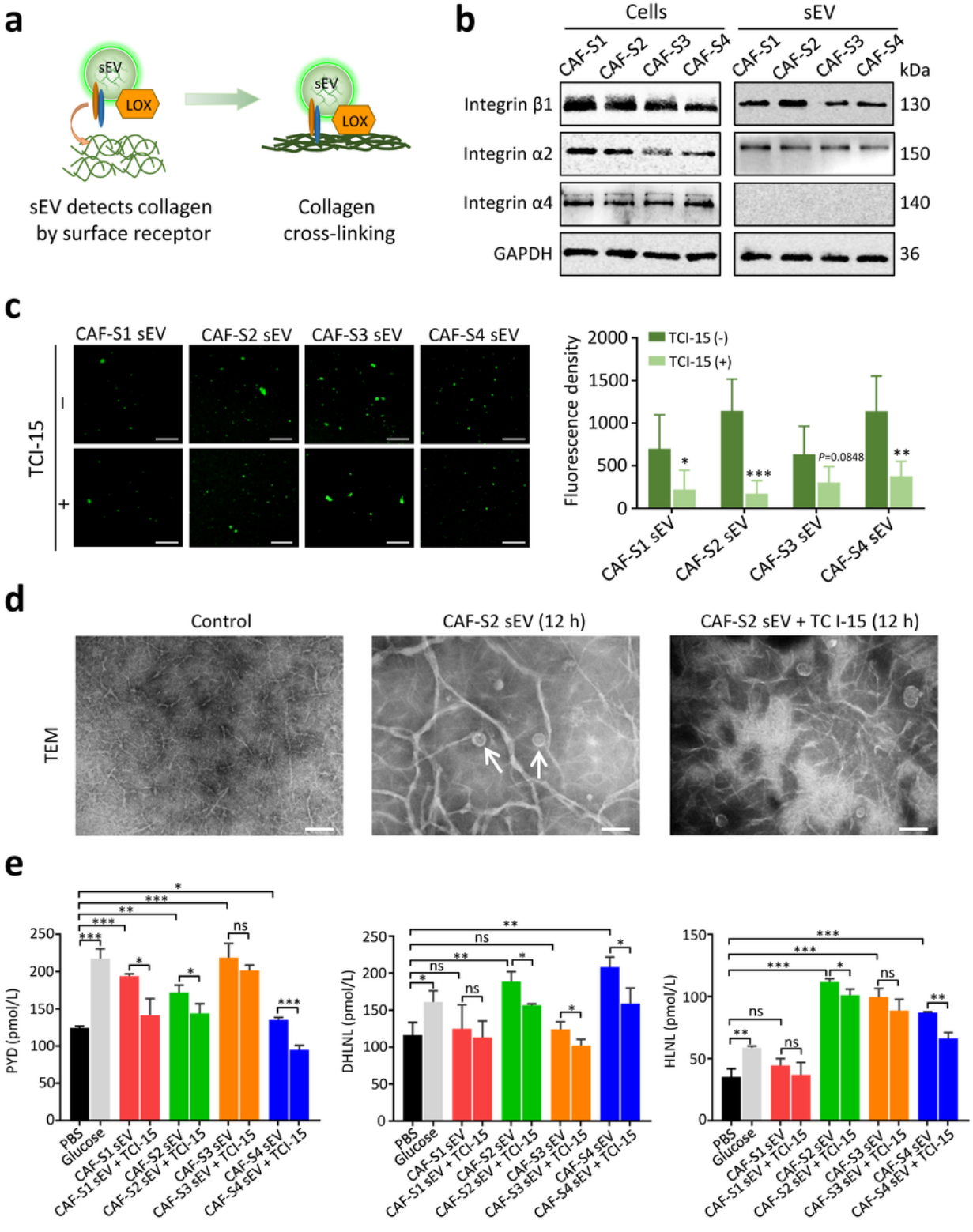

Figure 5

Collagen binding of CAF sEVs via integrin α2β1. (a) Schematic of collagen detection in CAF sEVs via the surface receptor. (b) Western blot analysis of integrin β1, α2, and α4 in CAF-S1/S2/S3/S4 cells and sEVs.

GAPDH was used as a control. (c) Inhibition of the binding of CAF-S1/S2/S3/S4 sEVs (green) to collagen I by treatment with TC I-15 *in vitro*. Left, representative images. Right, quantification results. Scale bar = 50 μm. (d) Representative TEM images of collagen crosslinking induced by CAF-S2 sEVs with or without TC I-15 treatment. PBS was used as a control. Thick collagen fibers associated with sEVs (arrows) were observed. Scale bar = 100 nm. (e) ELISA assay of PYD, DHLNL, and HLNL levels in the collagen matrix treated with CAF-S1/S2/S3/S4 sEVs with or without TC I-15. *$p < 0.05$, **$p < 0.01$, and ***$p < 0.001$.

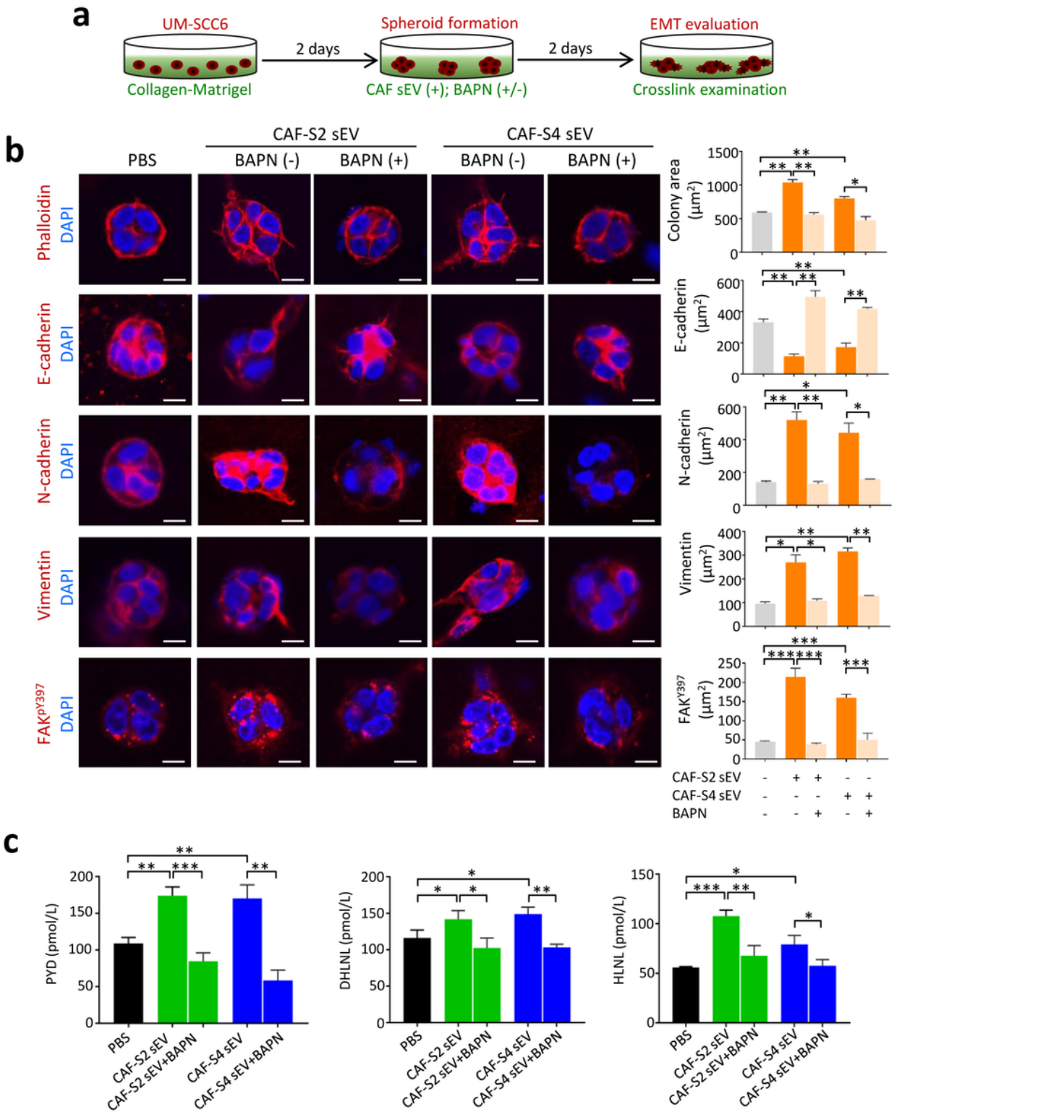

Figure 6

EMT of OSCC cells induced by CAF sEVs *in vitro*. (a) Illustration of collagen crosslinking in collagen-Matrigel mixture triggered by CAF sEVs and drive EMT of OSCC. (b) The morphology (phalloidin) and expression of E-cadherin, N-cadherin, vimentin, FAK^{Y397} in UM-SCC6 spheroids stimulated by CAF-S2/CAF-S4 sEVs with or without BAPN. PBS was used as a control. Left: Representative images. Scale bar = 10 μm. Right: Quantitative analyses of cell invasion (phalloidin) and the expression of E-cadherin, N-cadherin, and vimentin in UM-SCC6 spheroids under different experimental conditions. (c) ELISA of PYD, DHLNL, and HLNL in the Matrigel-collagen I matrix treated with CAF-S2/S4 sEVs with or without BAPN. *$p < 0.05$, **$p < 0.01$ and ***$p < 0.001$.

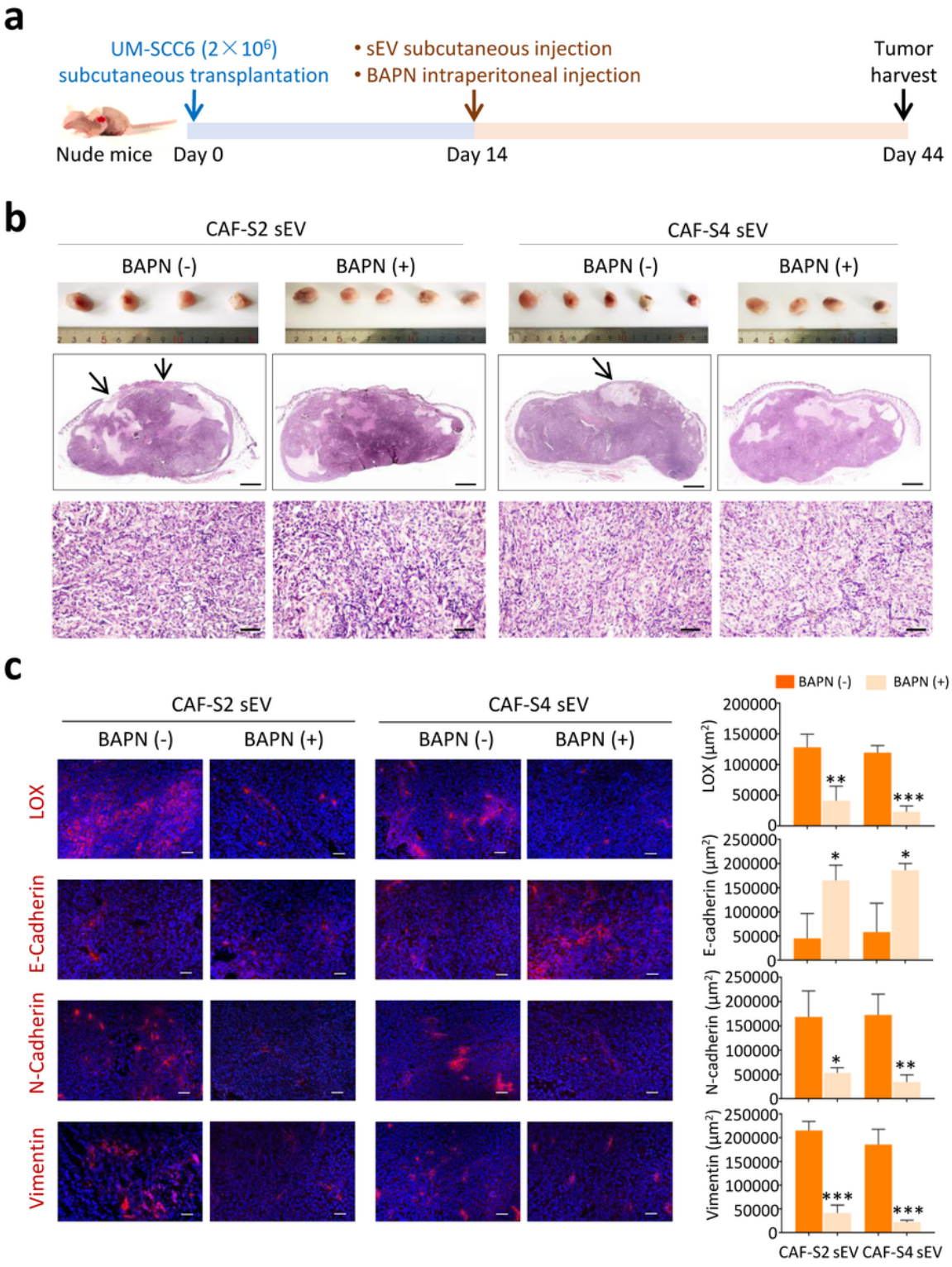

Figure 7

OSCC EMT induced by CAF sEVs *in vivo*. (a) Experimental steps. (b) Gross and histopathological examinations of UM-SCC6 xenografts treated with CAF-S2/S4 sEVs with or without BAPN (n = 5 per group). Scale bar = 100 μm. (c) Expression of LOX, E-cadherin, N-cadherin, and vimentin in UM-SCC6 xenografts. Left, representative images. Right, quantification results. Scale bar = 50 μm. *$p < 0.05$, **$p < 0.01$, ***$p < 0.001$.

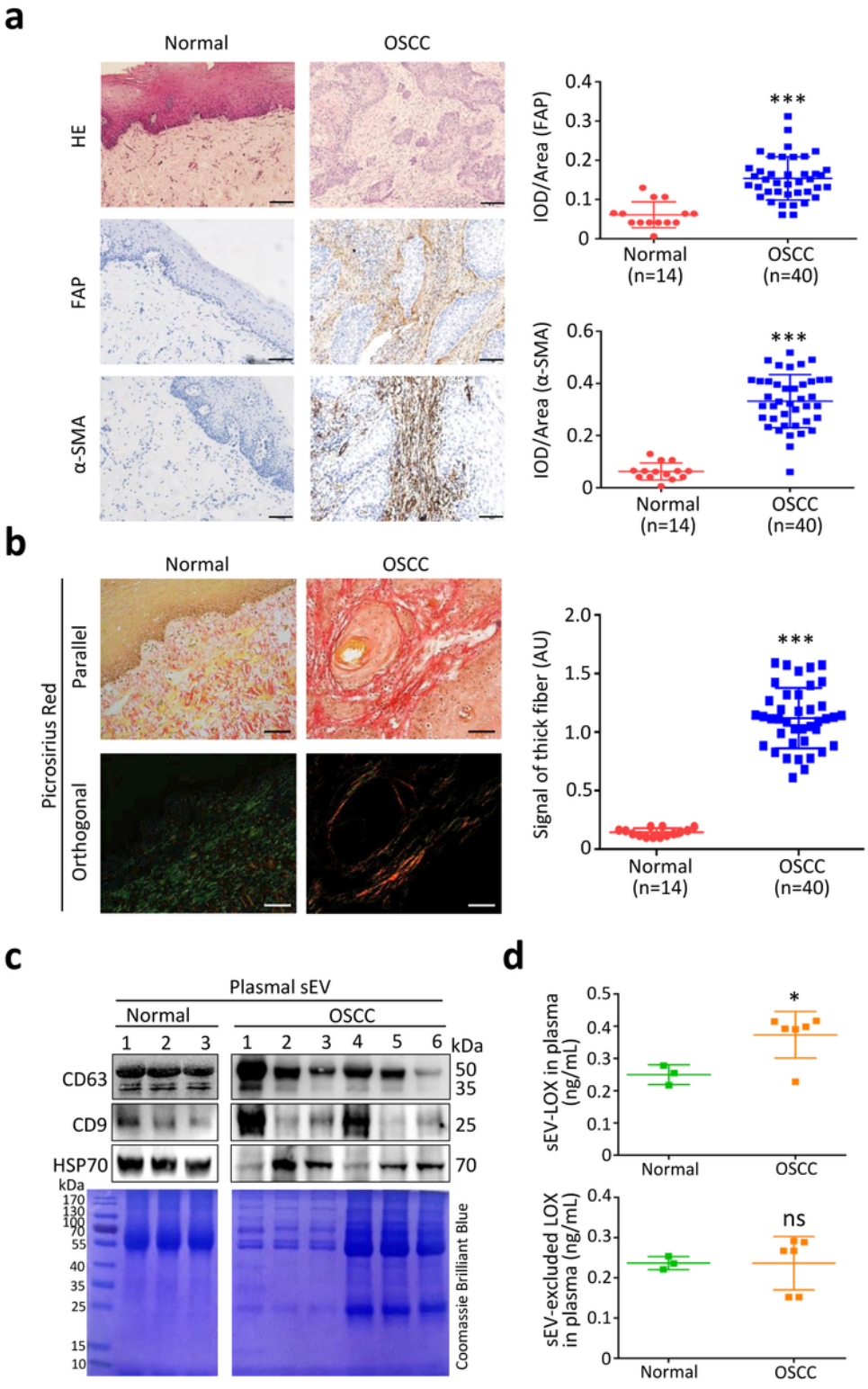

Figure 8

CAFs, collagen crosslinking, and sEV-LOX in OSCC stroma. (a) Expression of FAP and α-SMA, biomarkers of CAFs, in OSCC cases and normal controls. Left: Images of normal and OSCC tissues. Right: Quantification of FAP and α-SMA expression. Scale bars = 100 μm. (b) Collagen crosslinking evaluation by picrosirius red staining in normal and OSCC stroma. Left: Images viewed under parallel (top) and orthogonal polarizing filters (bottom). Right: Quantification of images viewed under orthogonal polarizing

filters. Scale bars = 50 μm. (c) Western blot analysis of CD63, CD9 and HSP70 in plasmal sEVs from 3 healthy controls and 6 OSCC patients. (d) ELISA analysis of plasmal sEV-LOX and sEV-excluded LOX in healthy controls and OSCC patients. ns, not significant, *$p < 0.05$, ***$p < 0.001$.

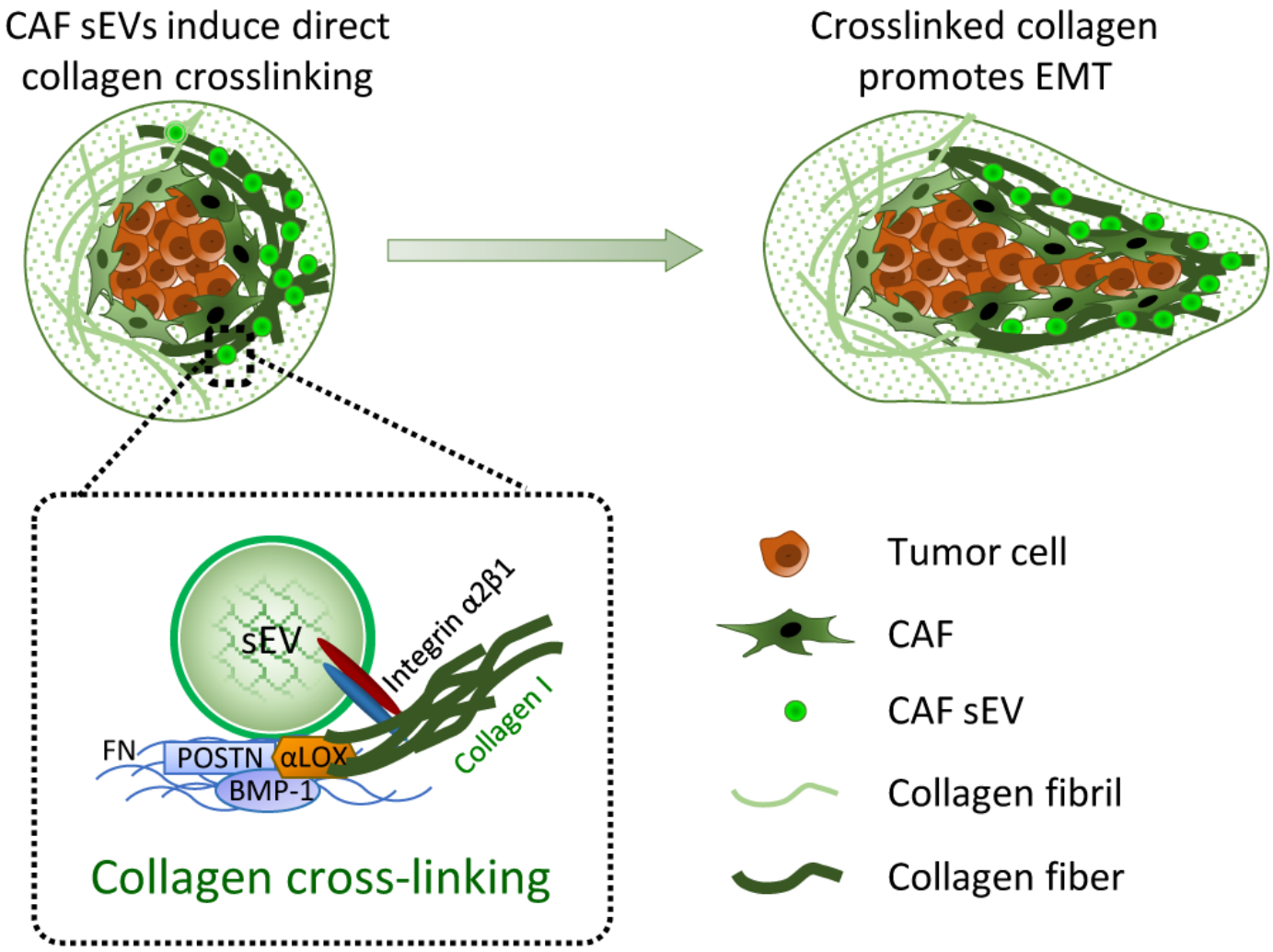

Figure 9

Schematic of collagen crosslinking triggered by CAF sEVs leading to EMT of OSCC. CAFs in the tumor microenvironment secrete sEVs enriched in α-LOX, which interact with FN, POSTN, and BMP-1. CAF sEVs detect collagen via integrin α2β1 and induce direct collagen crosslinking. The crosslinked matrix promotes EMT of OSCC cells.

Supplementary Files

This is a list of supplementary files associated with this preprint. Click to download.

- Supplementarymethods.docx

- SupplementaryFigures.docx
- Supplementarytables.docx